2015

An intensified seasonal transition in the Central U.S. that enhances summer drought

S.-Y. Simon Wang
Utah State University, simon.wang@usu.edu

Joseph Santanello
NASA Goddard Space Flight Center, Greenbelt, Maryland

Hailan Wang
NASA Goddard Space Flight Center, Greenbelt, Maryland,

Daniel Barandiaran
Utah State University

Rachel T. Pinker
University of Maryland

See next page for additional authors

AGU PUBLICATIONS

JGR

Journal of Geophysical Research: Atmospheres

RESEARCH ARTICLE
10.1002/2014JD023013

Key Points:
- Summer drying in Central U.S. has been enhanced
- Intensified spring-summer transition aggravated drought
- Land-atmosphere feedback increased the 2012 drought

Correspondence to:
S.-Y. S. Wang,
simon.wang@usu.edu

Citation:
Wang, S.-Y. S., et al. (2015), An intensified seasonal transition in the Central U.S. that enhances summer drought, *J. Geophys. Res. Atmos.*, *120*, 8804–8816, doi:10.1002/2014JD023013.

Received 22 DEC 2014
Accepted 29 JUL 2015
Accepted article online 1 AUG 2015
Published online 9 SEP 2015

An intensified seasonal transition in the Central U.S. that enhances summer drought

S.-Y. Simon Wang[1], Joseph Santanello[2], Hailan Wang[2], Daniel Barandiaran[1], Rachel T. Pinker[3], Siegfried Schubert[2], Robert R. Gillies[1], Robert Oglesby[4], Kyle Hilburn[5], Ayse Kilic[6], and Paul Houser[7]

[1]Utah Climate Center/Department of Plants, Soils and Climate, Utah State University, Logan, Utah, USA, [2]NASA Goddard Space Flight Center, Greenbelt, Maryland, USA, [3]Department of Atmospheric and Oceanic Science, University of Maryland, College Park, Maryland, USA, [4]Department of Earth and Atmospheric Sciences, University of Nebraska–Lincoln, Lincoln, Nebraska, USA, [5]Remote Sensing Systems, Santa Rosa, California, USA, [6]Department of Civil Engineering and School of Natural Resources, University of Nebraska–Lincoln, Lincoln, Nebraska, USA, [7]Department of Geography and Geoinformation Science, George Mason University, Fairfax, Virginia, USA

Abstract In the long term, precipitation in the Central U.S. decreases by 25% during the seasonal transition from June to July. This precipitation decrease has intensified since 1979 and such intensification could have enhanced spring drought occurrences in the Central U.S., in which conditions quickly evolve from being abnormally dry to exceptionally dry. Various atmospheric and land reanalysis data sets were analyzed to examine the trend in the June–July seasonal transition. The intensified deficit in precipitation is accompanied by increased downward shortwave radiation flux, tropospheric subsidence, enhanced evaporative fraction, and elevated planetary boundary layer height, all of which can lead to surface drying. The change in tropospheric circulation was characterized by an anomalous ridge over the western U.S. and a trough on either side—a pattern known to suppress rainfall in the Central U.S. This trending pattern shows similarity with the progression of the 2012 record drought.

1. Introduction

In the Central United States, the seasonal progression from June to July involves a climatological feature of rainfall reduction. Such rainfall reduction occurs in association with the development of the North American Monsoon (NAM) and concurrent formation of the upper level anticyclone over the western U.S., nudging the jet stream northward [*Barlow et al.*, 1998; *Higgins et al.*, 1997; *Wang and Chen*, 2009]. In summer 2012, the Central U.S. underwent a severe (record) drought. A unique feature of this drought was its rapid intensification during the early summer [*Hoerling et al.*, 2013a, 2013b]. Figure 1a, reproduced from *Hoerling et al.* [2013a], depicts the rapid expansion of drought conditions in Wyoming, Colorado, Kansas, Nebraska, and South/North Dakota. Over the period of just 1 month, the drought conditions worsened from moderate to severe status. The timing of this drought's rapid intensification coincides with a subseasonal feature in the Central U.S.: precipitation generally is reduced by about 25% from June to July, as shown in Figure 1b by the long-term monthly rainfall. The precipitation difference of July minus June, **denoted hereafter as "July–June,"** depicts a distinct zone of rainfall reduction to the north and east of the NAM region (Figure 2a) covering the Central Plains and the Great Plains. While this seasonal rainfall reduction is a well-known phenomenon, the extent to which a progression of drying may have changed has not been examined.

The extreme and widespread impacts of the 2012 record drought have prompted a number of recent studies, including those dealing with the meteorological processes and drought prediction [*Hoerling et al.*, 2013a; *Hoerling et al.*, 2013b; *Kumar et al.*, 2013], drought depiction using various monitoring tools [*Mallya et al.*, 2013], drought recovery [*Pan et al.*, 2013], low-frequency climate variability and trends [*Barandiaran et al.*, 2013; *Wang et al.*, 2014], impacts on agriculture and economy [*Al-Kaisi et al.*, 2013], and global food security [*Boyer et al.*, 2013]. The lack of prominent large-scale forcing factors in the tropics, such as that of El Niño–Southern Oscillation, was thought to be a probable reason for low skill in climate models' prediction of the 2012 drought [*Hoerling et al.*, 2013b; *Wang et al.*, 2014]. In this study, our goal is to examine other possible forcing factors, with emphasis on regional drivers and dynamical mechanisms that may be related to the rapid advancement and expansion of drought (such as that in 2012) including the role of land-atmosphere interactions, circulation patterns, their interaction, and, subsequently, how some or all of these may have changed.

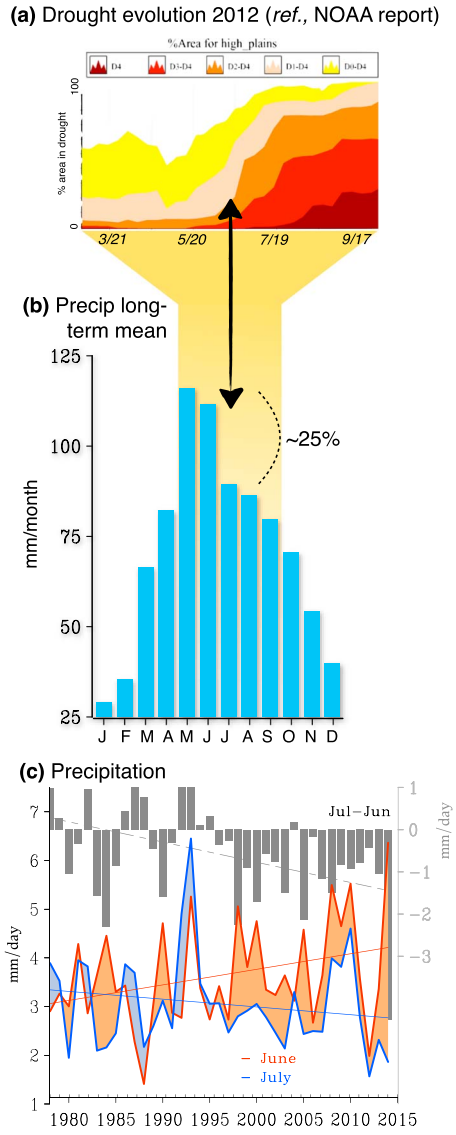

Figure 1. (a) Drought evolution during 2012 obtained from *Hoerling et al.* [2013a], showing the percent of areas under negative PDSI from March to September 2012. (b) Long-term (1971–2000) mean monthly precipitation in the Central Plains from the domain outlined in Figure 2a. (c) Time series of precipitation in June (blue), July (red), and the July-June difference (bar) from 1978 to 2014 overlaid with linear trends.

To accomplish our analysis, we utilized an array of surface observations and global reanalysis data sets; these are outlined in section 2. Surface conditions associated with the change in the June–July circulation transition are presented in section 3, followed by an analysis of the atmospheric and oceanic conditions in section 4. A climate model attribution analysis is presented and discussed in section 5. Concluding remarks are provided in section 6.

2. Data and Models

2.1. Data Sources

Global reanalysis products were adopted to support this study. However, any exploration of long-term changes using a single reanalysis is of concern due to inconsistent trends among different reanalyses [*Paltridge et al.*, 2009]. Thus, to obtain an optimal estimate of long-term trends in the atmosphere, we utilized an array of global reanalyses and sought consensus. We used four post-1979 data sets that cover the satellite era—the acronyms, full names, and description of each data set are provided in Table 1. The data group consists of Modern-Era Retrospective Analysis for Research and Applications (MERRA) [*Rienecker et al.*, 2011], Climate Forecast System Reanalysis (CFSR) [*Saha et al.*, 2010], ERA-Interim [*Dee et al.*, 2011], and the National Center for Environmental Prediction/Department of Energy (NCEP/DOE) "R-2" reanalyses [*Kanamitsu et al.*, 2002]. In the following analyses, the atmospheric variables are derived from an ensemble of these four reanalysis data sets using equal-weight averaging. In addition, the North American Regional Reanalysis (NARR) regional reanalysis data [*Mesinger et al.*, 2006] were used for the analysis of boundary layer heights. Other observational data sets included the monthly Climatic Research Unit (CRU) precipitation and surface air temperature data and the Palmer Drought Severity Index (PDSI) at 0.125°—derived from the Parameter-elevation Regressions on Independent Slopes Model (PRISM), as well as the NOAA Extended Reconstructed Sea Surface Temperature (SST) [*Smith et al.*, 2008] for the depiction of ocean states.

Land surface analyses were obtained from the Mosaic [*Koster and Suarez*, 1994] and Noah [*Ek et al.*, 2003] land surface models as part of the recently released North American Land Data Assimilation System project Phase 2 (NLDAS-2) [*Xia et al.*, 2012]. All land surface models were run offline at 0.125° horizontal resolution using gauge

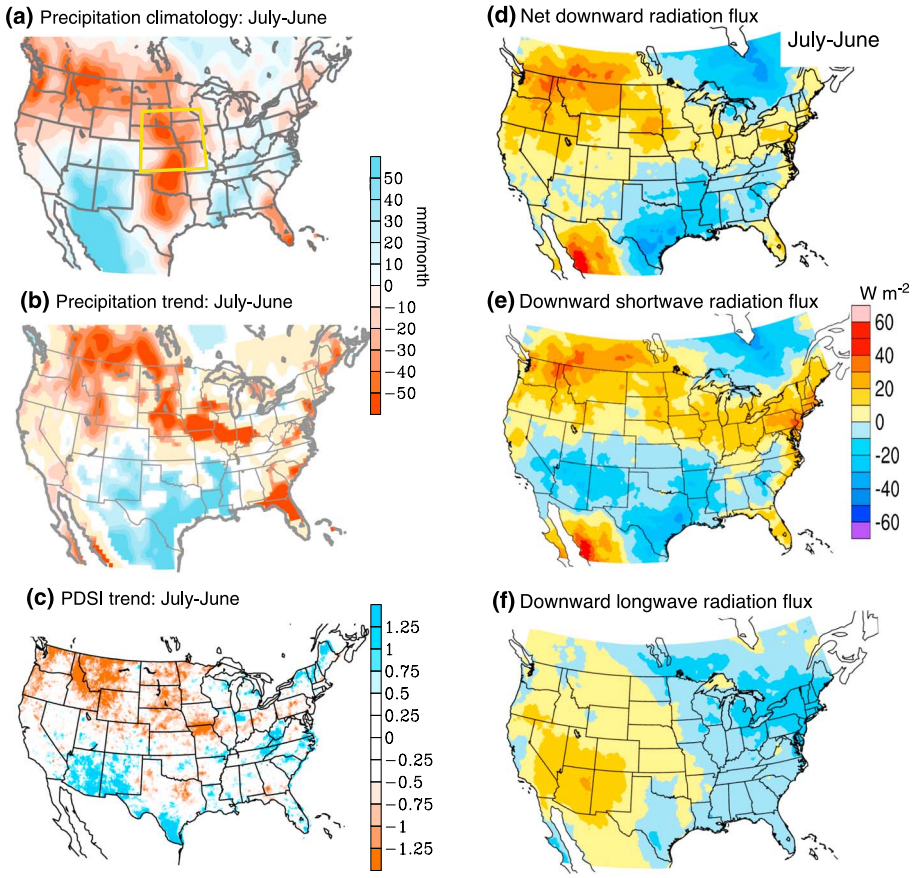

Figure 2. (a) Long-term mean of the July-June precipitation change; the yellow domain indicates the Central Plains and linear trends in the July-June difference of (b) precipitation (CRU data), (c) PDSI (PRISM data), (d) net downward radiation flux, (e) downward shortwave radiation flux, and (f) downward longwave radiation flux (NLDAS-2 data). In Figure 2b the red and blue colors indicate the significance at the 95% interval, while in Figure 2c only values significant at 90% are colored.

and bias-corrected atmospheric (NLDAS-2) forcing data. Monthly means were calculated across the period of record (1979–2012), while linear trends were calculated up to 2011 (to leave 2012 out for validation).

2.2. Model Simulations

To investigate the forcing sources of change in the June–July transition, we also examined a set of idealized model simulations using the NASA Goddard Earth Observing System model, version 5 (GEOS-5) atmospheric

Table 1. Global and Regional Reanalyses Used

Name	Full Name and Agency	Spatial Resolution
MERRA	Modern-Era Retrospective Analysis for Research and Applications, by the National Aeronautics and Space Administration (NASA)	1.0° longitude × latitude → extrapolated to 2.5°
ERA-Interim	European Centre for Medium-Range Weather Forecasts Interim Reanalysis project, by the European Centre for Medium-Range Weather Forecasts	1.5° longitude × latitude → extrapolated to 2.5°
CFSR	Climate Forecast System Reanalysis, by the National Oceanic and Atmospheric Administration (NOAA)	2.5° longitude × latitude
NCEP/DOE R-2	National Center for Environmental Prediction (NCEP)/ Department of Energy (DOE) Reanalysis, version 2	2.5° longitude × latitude
NARR	North American Regional Analysis, by NCEP	32 km horizontal grid

general circulation model (AGCM). The AGCM simulations consist of a control run forced with a seasonally varying SST climatology (1901–2004) and three anomaly runs forced with a warming trend pattern, a cold Pacific Decadal Oscillation (PDO) pattern, and a warm Atlantic pattern (superimposed onto the seasonally varying SST climatology). Following *Schubert et al*. [2009], the warming trend and Atlantic SST patterns were obtained as the first and third leading rotated empirical orthogonal function (REOF) modes of annual mean SST over the period of 1901–2004; the PDO SST pattern was obtained as the second leading REOF of low-pass filtered monthly SST data (1901–2004) that retain time scales of about 6 years and longer, following *Zhang et al.* [1997]. The amplitudes for the imposed PDO and Atlantic SST patterns were two standard deviations of their principal components, with the assumption of linear model response. The warming trend pattern used one standard deviation of its principal component and was used to simulate the impact of warming during the latter half of the twentieth century. All the GEOS-5 simulations were 50 years long. The model response to a leading SST pattern was obtained as the 50 year mean difference between the control run and the anomaly run. For these experiments, the GEOS-5 AGCM was run with 1° horizontal resolution on a latitude/longitude grid. *Schubert et al.* [2009] provides more details of the leading SST patterns and the AGCM experiment design. The GEOS-5 AGCM is described in *Rienecker et al.* [2008] and *Molod et al.* [2012], with the latter providing a comprehensive assessment of model fidelity. Moreover, we also utilized simulations produced by five AGCMs (Community Climate Model, Version 3 (CCM3); Community Atmospheric Model, Version 4 (CAM4); European Centre/Hamburg GCM model, Version 5 (ECHAM5); GEOS-5; and Global Forecast System (GFS)) that are part of the NOAA Facility for Climate Assessments (FACTS), which provided Atmospheric Model Intercomparison Project (AMIP) type of simulations (i.e., models were forced by prescribed/observed SST forcing) for the period of 1979–2012.

3. Surface and Planetary Boundary Layer Conditions

The linear trend of the 1979 to 2011 change in the July-June precipitation difference (i.e., July minus June) is shown in Figure 2b. In comparison with Figure 2a, the precipitation deficit in July has become greater in the Central Plains and northern Rockies. Indeed, there has been a twofold decrease in precipitation over Iowa, Nebraska, and portions of Illinois since the 1980s. In Figure 1c we plotted the evolutions of June and July precipitation and their difference over this area; it depicts a persistent reduction after 1995. Also noteworthy is the predominant increase in the June rainfall with a mild decrease in July that collectively enhances the July rainfall deficit. Likewise, the linear trend of the July-June PDSI difference (Figure 2c) indicates that drought conditions have intensified during the June–July transition over the Central Plains. A trend analysis conducted on the difference between the averages of May and June and July and August (not shown) also yielded a similar result in both precipitation and PDSI.

Another factor worth noting is the trend in the July-June net downward radiation flux at the surface (Figure 2d), derived from NLDAS-2 data. The positive trend in the downward radiation flux change reveals a pattern very similar to the negative trend in precipitation, i.e., meridionally elongated pattern with a particularly strong increase in the northern Great Plains. The pattern of net downward radiation flux results primarily from the change in downward shortwave radiation flux (Figure 2e) caused by change in cloud cover or cloud thickness. In comparison, the trend in the July-June downward longwave radiation (Figure 2f) depicts an east-west dipole pattern with increased radiation in the southwest and decreased radiation in the northeast. This indicates that the Central U.S. received either increased shortwave radiation in July or decreased radiation in June or a combination of both.

The impact of the downward radiation shift on the near-surface meteorology was examined by computing the trend in the 2 m air temperature ($T2$ m) for June (Figure 3a), (b) July (Figure 3b), and July-June (Figure 3c). In June, warming was observed over the Southwest U.S. and south of the U.S.-Mexico border, while a slight cooling is found in the northwest. In July, a distinct warming trend covers the entire Interior West. Therefore, the July-June change in $T2$ m depicts a marked warming centered around Idaho, Montana, and surrounding states (Figure 3c), i.e., not the Central Plains! The consequence is shown in Figure 3d by the seasonal evolution of thickness within 200 hPa and 700 hPa between the recent era (1996–2012) and the earlier era (1979–1995). The local air mass in July has evidently expanded, hence the increased rate of change in the thickness from June to July (bar graph). These results suggest that the regional warming over the western U.S. is accompanied by an upper air ridge formation. A stationary ridge in this vicinity is known to induce dry conditions over the Central Plains; this will be discussed further in section 4.

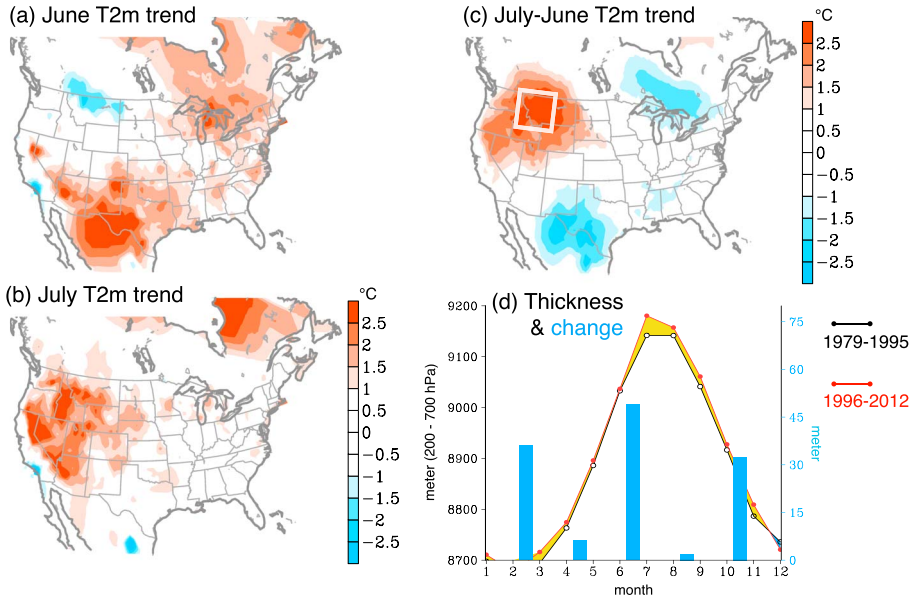

Figure 3. Trends in the 2 m air temperature (*T*2 m) for (a) June, (b) July, and (c) the July-June transition and (d) the thickness between 200 and 700 hPa averaged over the white outlined area in Figure 3c from the two periods as indicated and their monthly tendency shown as bars. The difference of thickness between the two periods is filled with yellow.

Next, we examined the changes in near-surface variables and the land-atmosphere coupling by computing the evaporative fraction (EF; Figure 4a), soil moisture in the near surface (top 40 cm; Figure 4b), and the planetary boundary layer (PBL) height (Figure 4c). EF is the ratio of evaporation flux to available energy, calculated as the difference between net radiation and soil heat flux. Here EF and soil moisture (SM) were derived from Mosaic model, and the PBL height was derived from NARR (we also analyzed the Noah model outputs, and the results were very similar in sign and spatial pattern.) The EF estimates are independent of precipitation inputs and generally do not reflect the influence of irrigation, which can substantially increase evapotranspiration rates. The linear trends of EF, soil moisture, and PBL variables were computed for June, July, and the July-June difference for the period of 1979–2011 and compared with the 2012 anomalies of the July-June difference; the "trends" in Figure 4 represent total change as the rate of change multiplied by the number of years from 1979 to 2011.

The decreasing trend in EF (Figure 4a) in the Central/Northern Great Plains indicates that there is a stronger transition in the primarily rain-fed surface energy balance from June to July. Further, it appears that soil moisture has mildly increased in June but subsequently decreased during July (Figure 4b); this echoes the observation by *Barandiaran et al.* [2013] that June has become significantly wetter in the Northern Plains while July has become slightly drier. A trend like this would increase the difference in EF between the 2 months, although the change is not so significant. In the Southern Great Plains (e.g., Oklahoma and especially southern Texas), the situation is reversed owing to an overall drying in the month of June and increased wetness in July. Both soil moisture and EF do show a drying trend in July in the Central Plains, a rather small area in the Nebraska/Iowa border. This rather small contribution of the drying trend on 2012 (Figure 4, bottom) suggests that surface processes alone may not be adequate for the long-term change to exacerbate drought; instead, the atmospheric processes should be taken into account, and this is discussed further next. Nevertheless, the fact that EF shows a stronger intensification in the July-June anomaly (than soil moisture) is supportive of the overall processes supporting the rapid onset of drought, as surface fluxes are more directly tied to the PBL feedback (in this case a rapid increase (decrease) in sensible (latent) heat flux). Further, the surface drying trend in July is also supported by increased PBL height as shown in Figure 4c. However, the translation of soil moisture to surface fluxes is not always direct and depends on many factors such as vegetation amount and evaporative physics, which may mask at times the direct connection of soil moisture to atmospheric impacts. This is why additional analysis was conducted for the atmospheric processes, shown later in Figures 5–7.

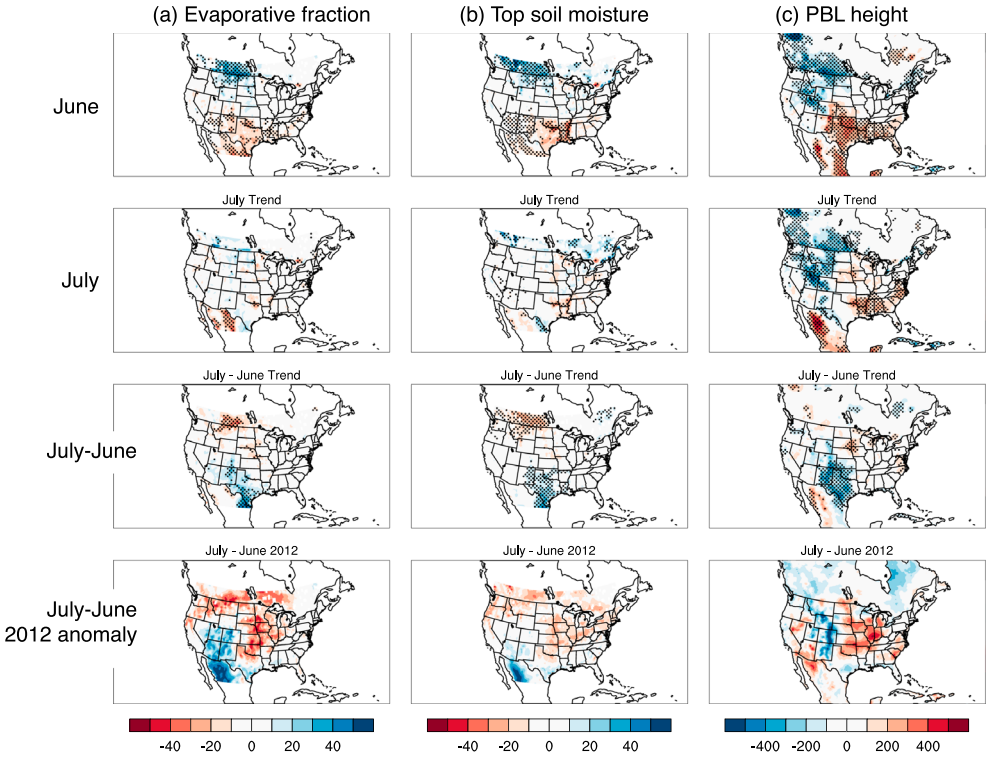

Figure 4. Linear trends calculated from 1979 to 2011 for (a) evaporative fraction (EF; % change), (b) shallow soil moisture at top 40 cm (SM; kg/m^2), and (c) PBL height (m) for (top to bottom) June, July, July-June, and the 2012 anomalies. The regression coefficients were multiplied by the number of years so values represent total change and not the rate of change. The dotted areas indicate the significance at the 95% interval per *t* test. EF and SM were derived from Mosaic model, and the PBL height was derived from NARR.

By comparing with the 2012 anomalies of the July-June EF, soil moisture, and the PBL height (Figure 4, bottom), it can be seen that the 2012 patterns are similar with those of the long-term trend. Surface drying and PBL growth from June to July 2012 are particularly pronounced over Kansas, Missouri, Illinois, and Indiana. An earlier analysis of satellite-derived greenness vegetation fraction from Moderate Resolution Imaging Spectroradiometer [*Wang et al*., 2014] also supports the observation that negative anomalies in vegetation amount and health were already present in summer 2012. Likewise, as was shown in a companion study, *Santanello et al.* [2015], the Atmospheric Radiation Measurement-Southern Great Plains Facility at Lamont, OK, observed a record increase in the PBL height during July. Apparently, the land-PBL feedback have tended to take hold more suddenly in recent years, leading to accelerated drying of the lower atmosphere, an increase in the PBL height and, as inferred from Figure 4c, an increased entrainment in July. *Cattiaux and Yiou* [2013] also indicated that, during 2012, the recorded high temperature and lack of rains in May played an important role in the later development of the drought through land surface processes. These processes can establish a deep residual boundary layer that promotes further desiccation of the soil. A positive feedback such as this, as well as its long-term intensification, is manifest in the greater July-June change in EF and the PBL in 2012.

4. Circulation Changes Versus Remote Forcing

As previously noted, the development of the NAM is associated with a noticeable transition in upper level circulations from the cold season regime (trough) to midsummer regime (ridge); this is illustrated in Figure 5. In June, a stationary trough near the West Coast characterizes the upper level circulation with the jet exit located over the Central Plains (Figure 5a). In July, the monsoonal anticyclone develops, pushing the jet stream northward to about 50°N (Figure 5b); consequently, the circulation forms an anticyclonic anomaly over the western U.S. (Figure 5c) from June to July, and this induces subsidence over the Central Plains

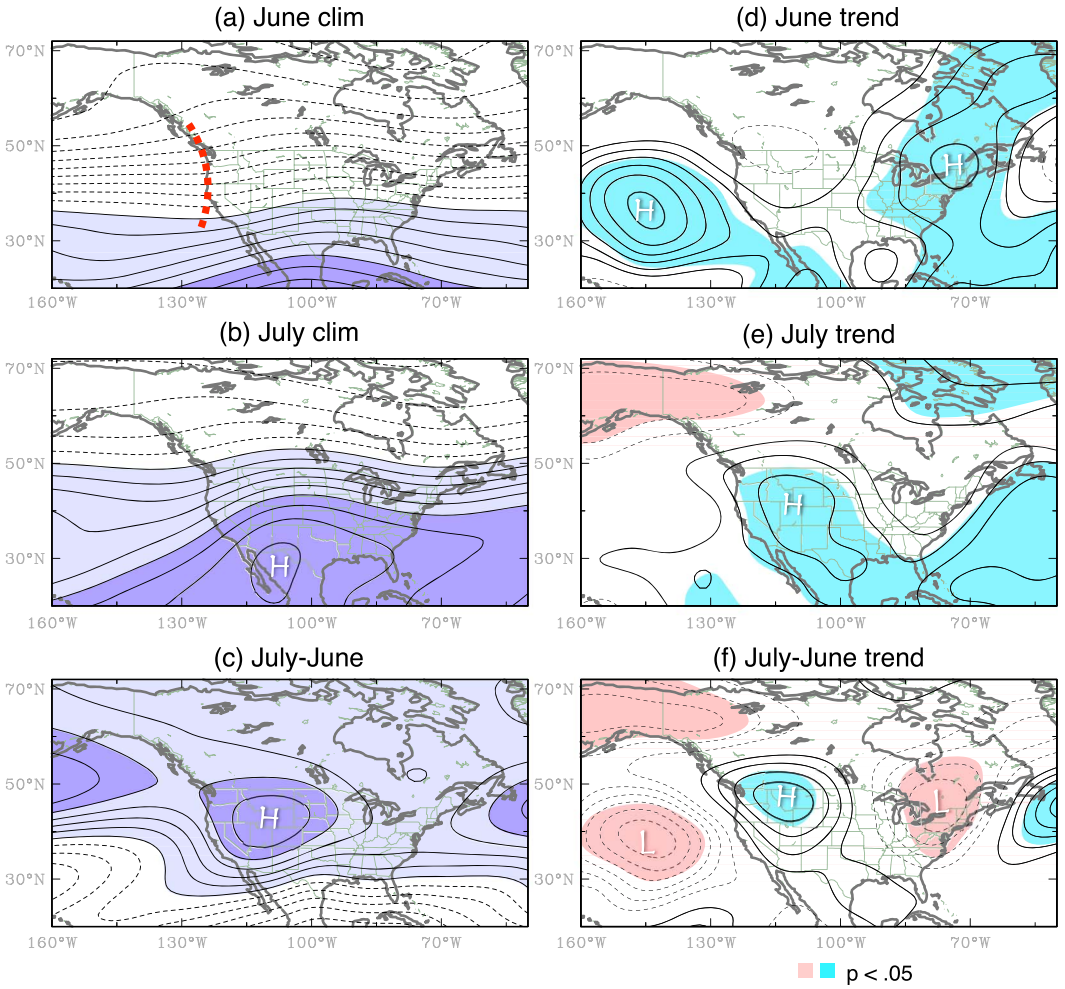

Figure 5. Mean stream function ($m^2\ s^{-1}$) at 200 hPa in (a) June, (b) July, and (c) July-June transition, with a contour interval of 5×10^6 in Figures 5a and 5b and 2.5×10^6 in Figure 5c. The 1979–2011 trends in stream function for (d) June, (e) July, and (f) July-June transition, with a contour interval of 1.5×10^6. These values are the slope of linear trends multiplied by the number of years from 1979 to 2011, indicating a total change. The shadings in Figures 5d–5f indicate the regression coefficients significant at the 95% confidence interval. The dashed line in Figure 5a indicates the stationary trough, while "H" and "L" indicates high- and low-pressure anomalies, respectively.

[*Barlow et al.*, 1998; *Higgins et al.*, 1997]. The linear trends in these circulations (Figures 5d–5f) reveal an intensification manifest as a deepened western trough in June and enhanced western ridge in July. As a result, the July-June shift in the circulation (Figure 5f) depicts an amplified ridge in the northwestern U.S. and a deepened trough in the northeastern U.S. The western ridge corresponds well with increased surface warming underneath and tropospheric thickening (Figure 3). Such a change in the circulation manifests as a distinct shortwave pattern that suppresses summer moisture in the Central U.S. [*Barlow et al.*, 2001; *Lau and Weng*, 2002; *Wang and Chen*, 2009; *Weaver and Nigam*, 2008].

As indicated by the trend in the July-June velocity potential at 200 hPa in Figure 6a, there is an increase in the upper level convergence over the Central U.S. Increased subsidence is illustrated by the significant increase in the downward velocity at 500 hPa (Figure 6b), suggesting increased drying and stabilization during the June–July transition. In 2012, the July-June velocity potential (Figure 6c) and downward velocity (Figure 6d) reveal a comparable pattern indicating enhanced subsidence over the Central Plains. Recall in Figure 3c that the maximum warming occurs in western Montana, not the Central Plains, suggesting that increased drying in the Central U.S. is not directly linked to surface warming. This observation corresponds to the amplified western ridge (Figure 5f) that causes midtropospheric subsidence over the Central Plains

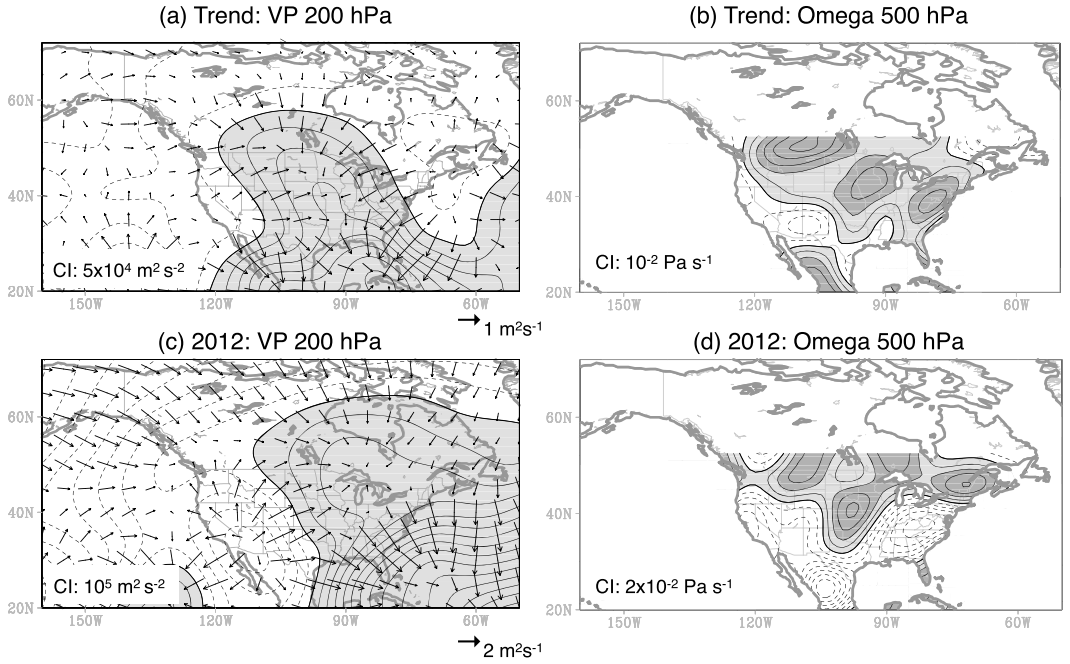

Figure 6. Same as Figure 5 but for the trends in the July-June (a) 200 hPa velocity potential (contours; $m^2 s^{-1}$) overlaid with divergent wind vectors ($m s^{-1}$) and (b) 500 hPa vertical velocity ($Pa s^{-1}$; positive is downward). (c and d) Same as Figures 6a and 6b but for the 2012 anomalies. Contour intervals are indicated at the lower left corner of each panel; unit vector is given in the lower right.

(Figure 6b) and resultant stabilization. Consistently, the largely negative trend in EF (Figure 4a) reflects the enhanced surface drying in July, and this indicates positive feedback that enhance drought conditions [*Cattiaux and Yiou*, 2013] after the atmospheric forcing took place. It was expected that subsidence over the Central U.S. must have strengthened correspondingly.

Summer anticyclonic anomalies in western North America are frequently connected to remote forcing in the North Pacific and Asia [*Newman and Sardeshmukh*, 1998; *Teng et al*., 2013]. Thus, to explore the climatic forcing of the circulation anomalies, Figure 7a displays the trends in the July-June SST and 200 hPa stream function: both reveal a remarkable similarity with the 2012 situation (Figure 7b). The distinct shortwave train across the midlatitudes implies a link with remote forcing that triggers a circumglobal teleconnection, from which Rossby wave energy propagates along the jet stream and affects North America [*Schubert et al*., 2011; *Teng et al*., 2013; *Wang et al*., 2014; *Wang et al*., 2013]. The weak tropical SST anomalies are also consistent with the notion for the lack of prominent tropical forcing in 2012 [*Hoerling et al*., 2013b; *Kumar et al*., 2013; *Wang et al*., 2014]. By comparison, trends in the June and July circulations and SST (Figures 7c and 7d) reveal a La Niña type of SST change in both months; this is also in agreement with previous studies analyzing the global SST trends [e.g., *Xie et al*., 2010]. While the circulation anomalies between the 2 months are quite different, neither month resembles any known teleconnection pattern.

The implication from Figure 7 is that the change in the July-June circulation evolution is not directly related to either the June or July SST anomalies but rather is related to the seasonal evolution of climatological SST (which determines atmospheric circulation forcing such as diabatic heating) and the tropospheric background flow (which directs atmospheric teleconnections). For example, given a diabatic heating anomaly in the tropics, the mean flow in June could still facilitate some Rossby wave propagation from the tropics to North America [*Newman and Sardeshmukh*, 1998], as is suggested in Figures 7c and 7d. However, the mean flow in July would prohibit such meridional propagation of Rossby waves but would instead facilitate zonally propagating short waves under the guidance of summer jets, as was previously documented [*Ding and Wang*, 2007; *Schubert et al*., 2011; *Wang et al*., 2010]. Likewise, an increase in regional warming over the Rocky Mountains (Figure 3b), which expands the middle troposphere, also can facilitate drying in the Central U.S. by inducing subsidence east of the ridge.

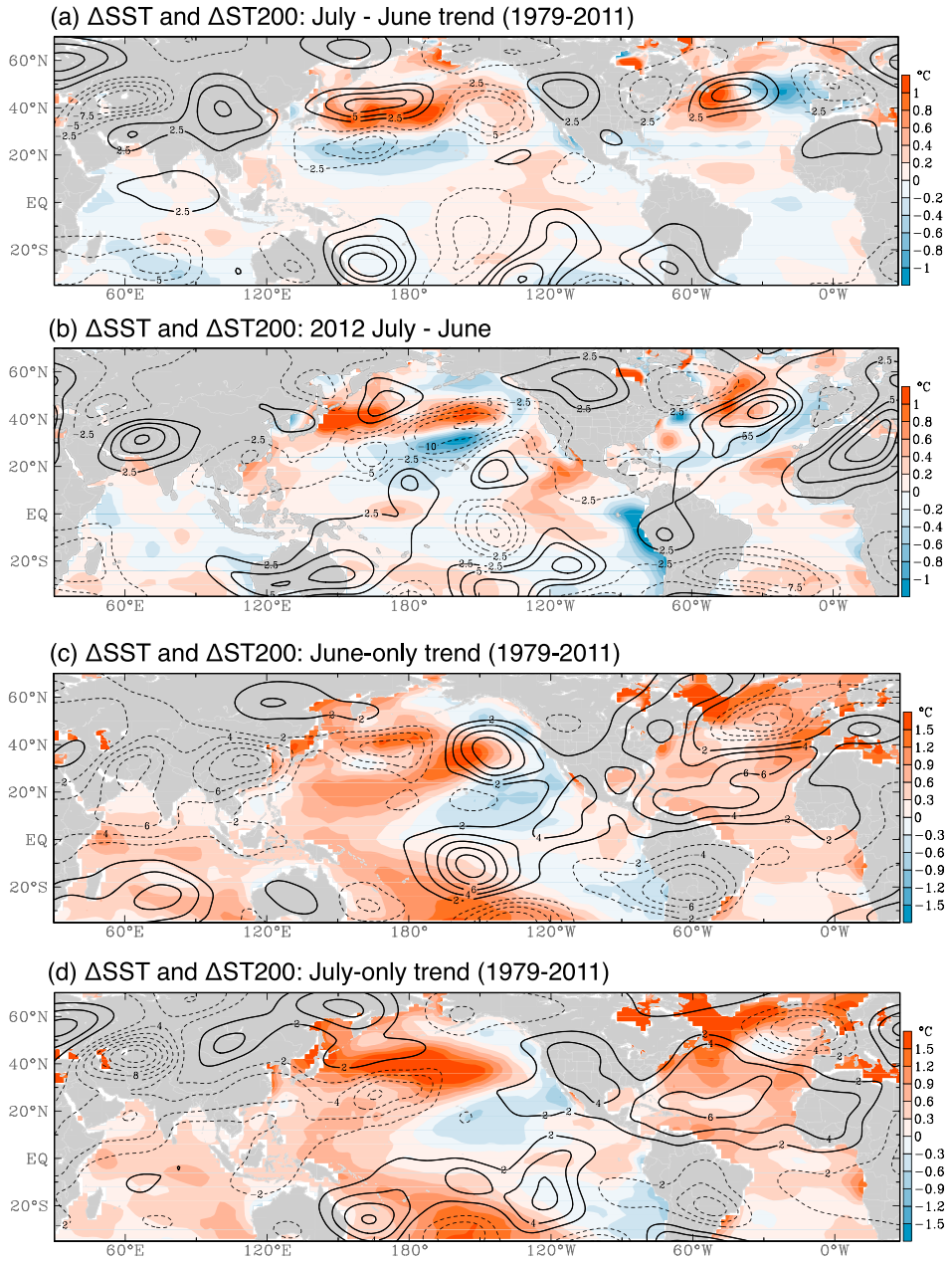

Figure 7. (a) The July-June changes in stream function at 200 hPa (contours) and SST (shadings) computed from the 1979–2011 trends. (b) Same as Figure 7a but for the 2014 anomalies. (c and d) Same as Figure 7a but for the trends for June and July, respectively. Zero contours of the stream function are omitted. Contour intervals are 2.5×10^6 m^2 s^{-1} in Figure 7a and 2×10^6 m^2 s^{-1} in Figures 7b and 7c. SST values exceeding ±0.9°C are generally significant at the 95% interval.

5. Climate Attribution

Previous studies have suggested that the trends in *T*2 m and precipitation over the U.S. are attributable to a combined contribution from phase changes of natural decadal-to-multidecadal oscillations, such as the Pacific Decadal Oscillation (PDO) and Atlantic Multidecadal Oscillation (AMO), in addition to global warming [*Robinson et al*., 2002; *Wang et al*., 2009; *Weaver et al*., 2009]. During the analysis period (1979–2012), the PDO in the late 1990s had shifted from the positive to negative phase; likewise the AMO had shifted from negative to positive phase, and the prominence of global warming has become increasingly so. Thus, to understand the extent to which the phase changes of PDO, AMO, and warming trend might have contributed to the

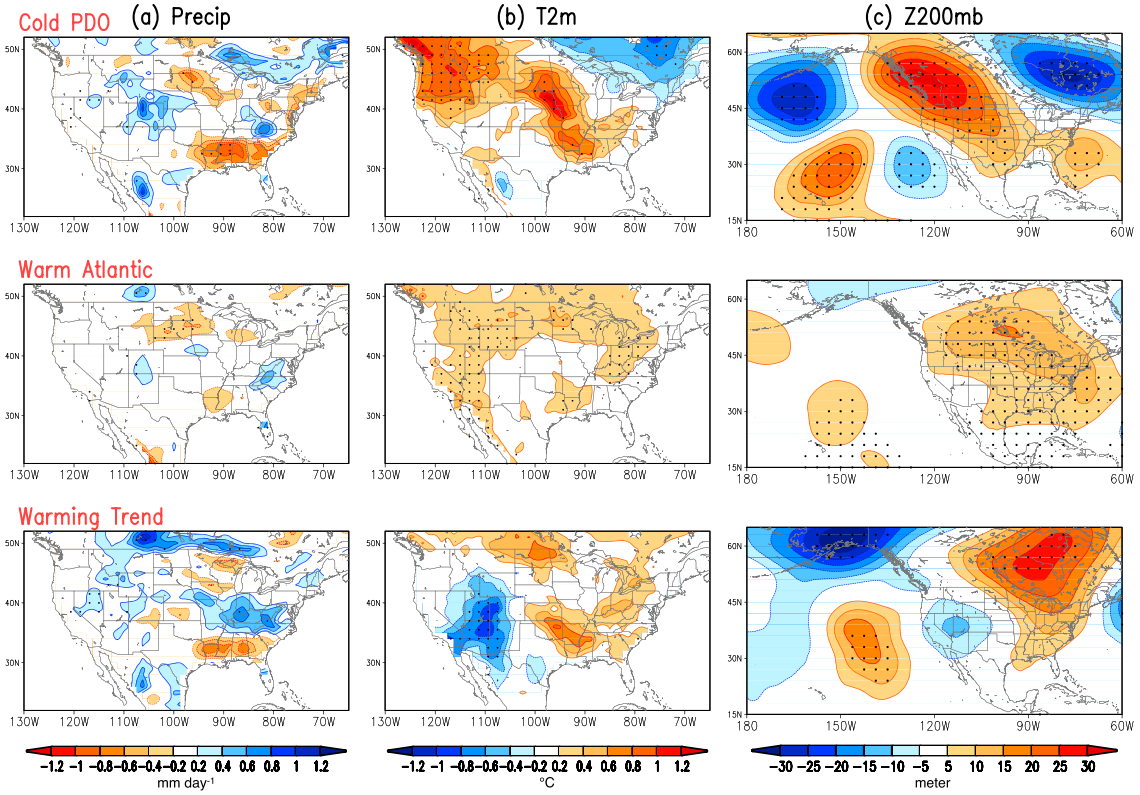

Figure 8. The GEOS-5 July-June responses of (a) precipitation (unit: mm/d), (b) surface air temperature (unit: K), and (c) geopotential height at 200 hPa (unit: m) to SST patterns of (top) a cold PDO, (middle) a warm Atlantic, and (bottom) a warm trend. The PDO SST pattern was obtained as the second leading rotated empirical orthogonal function (REOF) of low-pass filtered monthly SST data (1901–2004) that retain time scales of about 6 years and longer. The warm trend and Atlantic SST patterns were obtained as the first and third leading REOF modes of annual mean SST over the period of 1901–2004 [*Schubert et al.*, 2009]. The magnitudes of the model responses shown here correspond to SST forcing of two standard deviations. Stippling indicates significance at the 95% interval based on a *t* test.

observed change in the June–July transition, we undertook a set of idealized GEOS-5 AGCM experiments forced with three leading SST patterns: the cold PDO pattern (i.e., warmer SST in the central North Pacific), the warm Atlantic pattern, and the warming trend pattern (reference, section 2.2). These SST patterns, respectively, reflect the phase changes of the PDO and AMO during 1979–2012 and the global warming [*Schubert et al.*, 2009]. The responses of GEOS-5 AGCM to these SST patterns can be used to assess their relative contribution to the overall observed trends.

Figure 8 displays the AGCM responses of the July-June shifts in precipitation (Figure 8a), *T*2 m (Figure 8b), and 200 hPa geopotential height (Figure 8c) (In the midlatitudes under the quasi-geostrophic framework, stream function is proportional to geopotential height, and the two are used interchangeably). In terms of precipitation anomalies (Figure 8a), both cold PDO and warm Atlantic SST patterns force drying responses over Northern Plains. The effect of warming trend increases precipitation in the Central U.S., and this seems opposite to the cold PDO effect and observations. Note that most of the precipitation responses in the Central U.S. are not significant. Over the northwest U.S., the cold PDO pattern forced a pronounced surface warming and an anticyclonic anomaly (Figures 8b and 8c), along with a cooling and a cyclonic anomaly over the northeastern U.S., resembling the observed changes. Both the warm Atlantic and the warming trend produced a mild *T*2 m increase in the vicinity of the Central Plains accompanied by a weak ridge in the Central-eastern U.S. However, in the observation there is little to no warming in the Central Plains (Figure 3). The implication from these AGCM experiments is that the Pacific decadal variability (i.e., cold PDO) may contribute to the intensified June–July seasonal transition/drying, with secondary contributions coming from the Atlantic warming and the warming trend (similar to a La Niña response).

The result presented in Figure 8 raises the question whether or not AGCM simulations can provide convincing attribution in this case. A diagnosis like this depends on the model performance in reproducing the observed

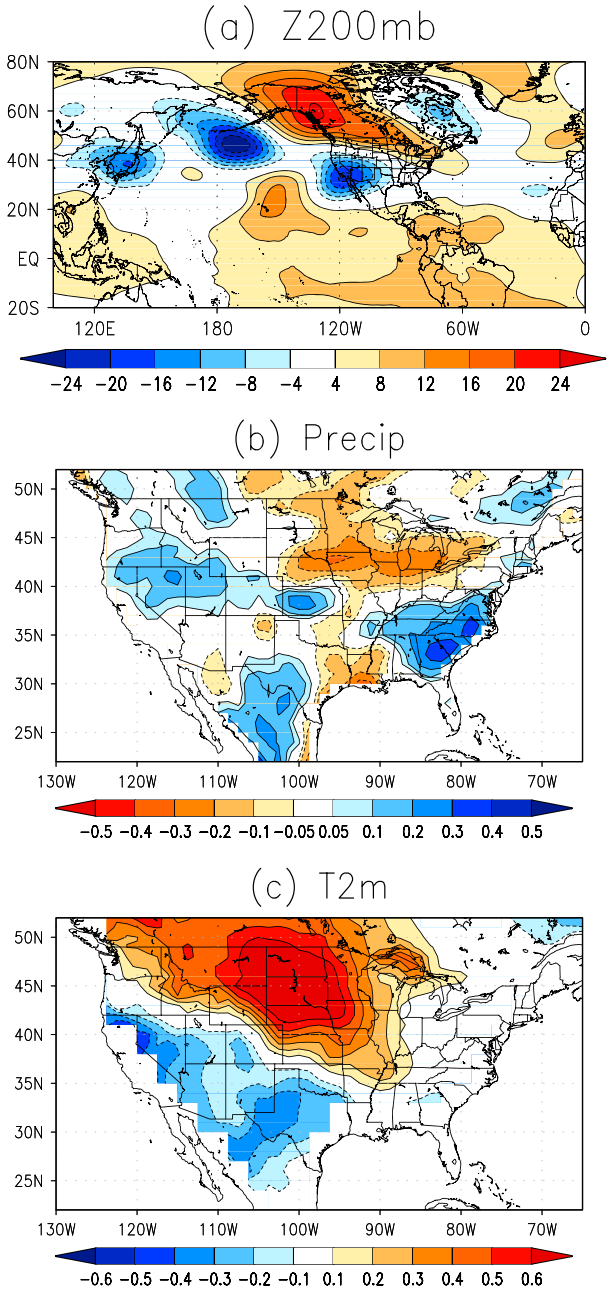

Figure 9. Five model ensembles (CCM3, CAM4, ECHAM5, GEOS-5, and GFS) of AMIP simulations for the 1979–2012 trends in the July-June (a) geopotential height at 200 hPa (unit: m), (b) precipitation (unit: mm/d), and (c) surface air temperature (unit: K).

July-June trend in their AMIP-style simulations (i.e., driven by prescribed SST forcing). Ideally, if a model can reproduce the observed July-June trend in its AMIP simulations, and if such model provides idealized AGCM runs forced with the leading SST patterns as discussed in Figure 8, then the comparison between its AMIP simulations and the idealized SST runs can indicate which leading SST pattern may play a role. The July-June change, however, is a second-order feature and is further challenging for any model, and the GEOS-5 model does not capture this feature well. To examine, Figure 9 shows the ensemble AMIP simulations by five AGCMs (CCM3, CAM4, ECHAM5, GEOS-5, and GFS included at FACTS; Xiao-Wei Quan 2014, personal communication). While the trend of July-June 200 hPa geopotential height shows some similarity to the observed (cf., Figure 5f), any longitudinal and latitudinal shifts of this modeled geopotential height from the observed—along with model handling of local land-atmosphere feedback—could lead to substantial model biases in precipitation and surface temperature anomalies. This is illustrated by the ensemble simulations of precipitation change (Figure 9b) and temperature change (Figure 9c), which together reveal an intensification of the July-June transition with a noticeable shift in the drying/warming pattern compared to the observation.

6. Concluding Remarks

Climatologically, precipitation in the Central U.S. decreases by about 25% during the June–July seasonal transition. Since 1979, this precipitation reduction has become greater, with decreases of 50% in recent years. At the larger scale, examination of tropospheric circulation change indicated that synoptic forcing was present and that it enhanced subsidence in the Central U.S., suppressing rainfall. Such a long-term change has a potential effect to aggravate droughts that develop in spring. In particular, the analyses presented here indicated a marked resemblance between the shifting June–July PDSI, precipitation, temperature, and circulation in the long term and those during the 2012 drought—one which was characterized by a rapid expansion over the Central Plains in mid-summer. As far as drought development is concerned, one important factor revealed from this study was land-atmosphere feedback that is caused by enhanced anticyclonic anomalies stationed over the western U.S. leading to further reductions in precipitation

and soil moisture in the Central U.S. In turn, the long-term changes in land surface moisture and evaporation can either sustain or amplify the subsidence and stabilization, further reducing precipitation. In the long run, land surface feedback to the atmospheric circulation anomalies is strong and can affect future drought expansion or development in the Central U.S. Understanding these processes can help anticipate the evolution and extent of drought in the Central U.S., especially those that occur in spring and prolong into summer. The next important task is to evaluate climate forecast models for the depiction of such seasonal transition during or prior to the occurrences of drought. The challenge of climate models lies in that they not only need to simulate the climate mean state and its linear trends correctly for June and July but also to depict the differences between these 2 months to regional details.

Acknowledgments

This study was partially supported by the NASA Energy and Water cycle Study. S. Schubert and H. Wang acknowledge support of the NASA MAP Program. Global reanalysis products are provided at http://gmao.gsfc.nasa.gov/research/merra/, http://cfs.ncep.noaa.gov/cfsr/, http://www.ecmwf.int/en/research/climate-reanalysis/era-interim, http://www.esrl.noaa.gov/psd/data/reanalysis/reanalysis.shtml, and http://www.esrl.noaa.gov/psd/data/gridded/data.narr.html. CRU precipitation and surface air temperature data are provided at http://www.cru.uea.ac.uk/data/, while the PDSI derived from PRISM is provided at http://www.wrcc.dri.edu/wwdt/batchdownload.php. NLDAS-2 data are provided at http://ldas.gsfc.nasa.gov/nldas/NLDAS2forcing.php. Model AMIP simulations of FACTS are provided at http://www.esrl.noaa.gov/psd/repository/alias/facts/.

References

Al-Kaisi, M. M., et al. (2013), Drought impact on crop production and the soil environment: 2012 experiences from Iowa, *J. Soil Water Conserv.*, *68*(1), 19A–24A.

Barandiaran, D., S.-Y. Wang, and K. Hilburn (2013), Observed trends in the Great Plains low-level jet and associated precipitation changes in relation to recent droughts, *Geophys. Res. Lett.*, *40*, 6247–6251, doi:10.1002/2013GL058296.

Barlow, M., S. Nigam, and E. H. Berbery (1998), Evolution of the North American Monsoon System, *J. Clim.*, *11*(9), 2238–2257.

Barlow, M., S. Nigam, and E. Berbery (2001), ENSO, Pacific decadal variability, and U.S. summertime precipitation, drought, and stream flow, *J. Clim.*, *14*(9), 2105–2128.

Boyer, J., P. Byrne, K. Cassman, M. Cooper, D. Delmer, T. Greene, F. Gruis, J. Habben, N. Hausmann, and N. Kenny (2013), The U.S. drought of 2012 in perspective: A call to action, *Global Food Secur.*, *2*(3), 139–143.

Cattiaux, J., and P. Yiou (2013), Explaining extreme events of 2012 from a climate perspective—Ch. 4: U.S. heat waves of spring and summer 2012 from the flow-analogue perspective, *Bull. Am. Meteorol. Soc.*, *94*(9), S1–S74.

Dee, D. P., et al. (2011), The ERA-Interim reanalysis: Configuration and performance of the data assimilation system, *Q. J. R. Meteorol. Soc.*, *137*(656), 553–597.

Ding, Q., and B. Wang (2007), Intraseasonal teleconnection between the summer Eurasian wave train and the Indian monsoon, *J. Clim.*, *20*(15), 3751–3767.

Ek, M., K. Mitchell, Y. Lin, E. Rogers, P. Grunmann, V. Koren, G. Gayno, and J. Tarpley (2003), Implementation of Noah land surface model advances in the National Centers for Environmental Prediction operational mesoscale Eta model, *J. Geophys. Res.*, *108*(D22), 8851, doi:10.1029/2002JD003296.

Higgins, R. W., Y. Yao, and X. L. Wang (1997), Influence of the North American Monsoon System on the U.S. summer precipitation regime, *J. Clim.*, *10*(10), 2600–2622.

Hoerling, M., et al. (2013a), An interpretation of the origins of the 2012 Central Great Plains drought, edited by NOAA/CPO/MAPP, 44 pp. [Available at http://cpo.noaa.gov/ClimatePrograms/ModelingAnalysisPredictionsandProjections/MAPPTaskForces/DroughtTaskForce/2012CentralGreatPlainsDrought.aspx.]

Hoerling, M., J. Eischeid, A. Kumar, R. Leung, A. Mariotti, K. Mo, S. Schubert, and R. Seager (2013b), Causes and predictability of the 2012 Great Plains drought, *Bull. Am. Meteorol. Soc.*, doi:10.1175/BAMS-D-13-00055.1.

Kanamitsu, M., W. Ebisuzaki, J. Woollen, S.-K. Yang, J. J. Hnilo, M. Fiorino, and G. L. Potter (2002), NCEP–DOE AMIP-II reanalysis (R-2), *Bull. Am. Meteorol. Soc.*, *83*(11), 1631–1643.

Koster, R. D., and M. J. Suarez (1994), The components of a "SVAT" scheme and their effects on a GCM's hydrological cycle, *Adv. Water Resour.*, *17*(1), 61–78.

Kumar, A., M. Chen, M. Hoerling, and J. Eischeid (2013), Do extreme climate events require extreme forcings?, *Geophys. Res. Lett.*, *40*, 3440–3445, doi:10.1002/grl.50657.

Lau, K.-M., and H. Weng (2002), Recurrent teleconnection patterns linking summertime precipitation variability over East Asia and North America, *J. Meteorol. Soc. Jpn.*, *80*(6), 1309–1324.

Mallya, G., L. Zhao, X. Song, D. Niyogi, and R. Govindaraju (2013), 2012 Midwest drought in the United States, *J. Hydrol. Eng.*, *18*(7), 737–745.

Mesinger, F., et al. (2006), North American regional reanalysis, *Bull. Am. Meteorol. Soc.*, *87*(3), 343–360.

Molod, A., L. Takacs, M. J. Suarez, J. Bacmeister, I.-S. Song, and A. Eichmann (2012), The GEOS-5 atmospheric general circulation model: Mean climate and development from MERRA to Fortuna Rep., 117 pp., NASA TM—2012-104606.

Newman, M., and P. D. Sardeshmukh (1998), The impact of the annual cycle on the North Pacific/North American response to remote low-frequency forcing, *J. Atmos. Sci.*, *55*(8), 1336–1353.

Paltridge, G., A. Arking, and M. Pook (2009), Trends in middle- and upper-level tropospheric humidity from NCEP reanalysis data, *Theor. Appl. Climatol.*, *98*(3), 351–359.

Pan, M., X. Yuan, and E. F. Wood (2013), A probabilistic framework for assessing drought recovery, *Geophys. Res. Lett.*, *40*, 3637–3642, doi:10.1002/grl.50728.

Rienecker, M. M., et al. (2008), The GEOS-5 data assimilation system—Documentation of versions 5.0.1, 5.1.0, and 5.2.0. Rep., 95 pp., NASA/TM-2007-104606.

Rienecker, M. M., et al. (2011), MERRA: NASA's Modern-Era Retrospective Analysis for Research and Applications, *J. Clim.*, *24*(14), 3624–3648.

Robinson, W. A., R. Reudy, and J. E. Hansen (2002), General circulation model simulations of recent cooling in the East-Central United States, *J. Geophys. Res.*, *107*(D24), 4748, doi:10.1029/2001JD001577.

Saha, S., et al. (2010), The NCEP Climate Forecast System Reanalysis, *Bull. Am. Meteorol. Soc.*, *91*(8), 1015–1057.

Santanello, S. A., Jr., J. Roundy, and P. A. Dirmeyer (2015), Quantifying the land–atmosphere coupling behavior in modern reanalysis products over the U.S. Southern Great Plains, *J. Clim.*, *28*, 5813–5829.

Schubert, S., et al. (2009), A U.S. CLIVAR project to assess and compare the responses of global climate models to drought-related SST forcing patterns: Overview and results, *J. Clim.*, *22*(19), 5251–5272.

Schubert, S., H. Wang, and M. Suarez (2011), Warm season subseasonal variability and climate extremes in the Northern Hemisphere: The role of stationary Rossby waves, *J. Clim.*, *24*, 4773–4792.

Smith, T. M., R. W. Reynolds, T. C. Peterson, and J. Lawrimore (2008), Improvements to NOAA's historical merged land–ocean surface temperature analysis (1880–2006), *J. Clim.*, *21*(10), 2283–2296.

Teng, H., G. Branstator, H. Wang, G. A. Meehl, and W. M. Washington (2013), Probability of U.S. heat waves affected by a subseasonal planetary wave pattern, *Nat. Geosci.*, *6*(12), 1056–1061.

Wang, H., S. Schubert, M. Suarez, J. Chen, M. Hoerling, A. Kumar, and P. Pegion (2009), Attribution of the seasonality and regionality in climate trends over the United States during 1950–2000, *J. Clim.*, *22*(10), 2571–2590.

Wang, H., S. Schubert, R. Koster, Y.-G. Ham, and M. Suarez (2014), On the role of SST forcing in the 2011 and 2012 extreme U.S. heat and drought: A study in contrasts, *J. Hydrometeorol.*, *15*, 1255–1273.

Wang, S.-Y., and T.-C. Chen (2009), The late-spring maximum of rainfall over the U.S. Central Plains and the role of the low-level jet, *J. Clim.*, *22*(17), 4696–4709.

Wang, S.-Y., L. E. Hipps, R. R. Gillies, X. Jiang, and A. L. Moller (2010), Circumglobal teleconnection and early summer rainfall in the U.S. Intermountain West, *Theor. Appl. Climatol.*, *102*, 245–252.

Wang, S.-Y., R. E. Davies, and R. R. Gillies (2013), Identification of extreme precipitation threat across midlatitude regions based on short-wave circulations, *J. Geophys. Res. Atmos.*, *118*, 11,059–11,074, doi:10.1002/jgrd.50841.

Wang, S.-Y., D. Barandiaran, K. Hilburn, P. Houser, B. Oglesby, M. Pan, R. Pinker, J. Santanello, S. Schubert, and H. Wang (2014), Could the 2012 drought in central U.S. have been anticipated? — A review of NASA working group research, *J. Earth Sci. Eng.*, *4*, 428–437.

Weaver, S. J., and S. Nigam (2008), Variability of the Great Plains low-level jet: Large-scale circulation context and hydroclimate impacts, *J. Clim.*, *21*(7), 1532–1551.

Weaver, S. J., S. Schubert, and H. Wang (2009), Warm season variations in the low-level circulation and precipitation over the Central United States in observations, AMIP simulations, and idealized SST experiments, *J. Clim.*, *22*(20), 5401–5420.

Xia, Y., et al. (2012), Continental-scale water and energy flux analysis and validation for the North American Land Data Assimilation System project Phase 2 (NLDAS-2): 1. Intercomparison and application of model products, *J. Geophys. Res.*, *117*, D03109, doi:10.1029/2011JD016048.

Xie, S.-P., C. Deser, G. A. Vecchi, J. Ma, H. Teng, and A. T. Wittenberg (2010), Global warming pattern formation: Sea surface temperature and rainfall*, *J. Clim.*, *23*(4), 966–986.

Zhang, Y., J. M. Wallace, and D. S. Battisti (1997), ENSO-like interdecadal variability: 1900–93, *J. Clim.*, *10*(5), 1004–1020.